Z. Phys. C - Particles and Fields 51, 341-350 (1991)

Zeitschrift für Physik C Particles and Fields


# Limits on neutral light scalar and pseudoscalar particles in a proton beam dump experiment

J. Blümlein, J. Brunner, H.J. Grabosch*, P. Lanius, S. Nowak, C. Rethfeldt, H.E. Ryseck, M. Walter
Institute for High Energy Physics, Zeuthen, Federal Republic of Germany

D. Kiss, Z. Jaki*
Central Research Institute of the Hungarian Academy of Sciences, Budapest, Hungary

L.S. Barabash, S.A. Baranov, Y.A. Batusov, S.A. Bunyatov, O.Y. Denisov, N.V. Gorbunov, A.G. Karev, M.Y. Kasarinov, O.L. Klimov, O.M. Kuznetsov, E.A. Ladygin, V.V. Lyukov, P.V. Mojsenz, V.P. Obudovski, S.N. Prakhov, V.I. Snyatkov
Joint Institute for Nuclear Research, Dubna, USSR

V.B. Anykeyev, N.S. Bamburov, A.A. Borisov, N.I. Boshko, A.P. Bugorsky, S.K. Chernishenko, G.L. Chukin, R.M. Fachrutdinov, N.A. Galjaev, V.N. Goryachev, M.M. Kirsanov, A.S. Koshin, V.I. Kravtsov, A.V. Kulikov, V.V. Lipajev, A.I. Mukhin, S.A. Mukhin, V.N. Ryshenkov, Y.I. Salomatin, Y.M. Sapunov, V.A. Senko, K.E. Shestermanov, A.A. Spiridonov, A.N. Sytin, V.V. Sytnik, V.A. Tumakov, A.S. Vovenko, V.P. Zhigunov, Y.A. Zudin
Institute for High Energy Physics, Serpukhov, USSR

Received 21 January 1991

**Abstract.** A search has been performed for weakly interacting neutral light scalar and pseudoscalar particles in a proton beam dump experiment. No positive signal is observed. Limits on the mass and life-time of these particles are set in the frame of the Standard Model and its minimal supersymmetric extension. The Higgs particle of the $SU_{2L} \times U_1$ Standard Theory is excluded for masses in the range 1 MeV $< m_H <$ 80 MeV at 95% CL. Limits on the Peccei-Quinn like axions are derived.

## 1 Introduction

In gauge theories with spontaneously broken symmetries weakly interacting neutral spin 0 bosons play a fundamental role. A scalar particle appears as a consequence of the Higgs mechanism [1] which is responsible for the masses of quarks, leptons and gauge bosons in the Standard Model (SM). In the minimal supersymmetric extension of the Standard Model (MSSM), two Higgs doublets exist which produce three neutral (pseudo)scalar particles. Two of them (one scalar $H$ and one pseudoscalar $A$) may be light [2]. In a similar way the axion was introduced by Peccei and Quinn [3] to solve the strong CP problem [4].

The direct finding of these particles would be very important for a proof of these mechanisms. From theory still only weak constraints for the mass of the Higgs boson exist. Assuming the absence of a strongly interacting Higgs sector, an upper mass limit of $M_H < 1$ TeV is introduced [5], but there are no simple restrictions for lower masses. For masses far below the electro-weak scale various searches have been performed [6-9] but so far no positive evidence has been found.

The interaction of these particles with fermions $f$ can be described by the following Lagrangians where the Higgs particle of the SM appears as a special case of the scalar $H$ and the axion as a special case of the pseudoscalar $A$

$$\mathscr{L}_{Hff} = \sum_f g_{Hf} f \bar{f} H, \tag{1.1}$$

$$\mathscr{L}_{Aff} = \sum_f g_{Af} f \gamma_5 \bar{f} A, \tag{1.2}$$

with the couplings

$$g_{Hf} = \mathrm{i} (\sqrt{2}\, G_F)^{1/2} m_f s_f,$$

$$g_{Af} = \mathrm{i} (\sqrt{2}\, G_F)^{1/2} m_f p_f.$$

* Present address: Joint Institute for Nuclear Research, Dubna, USSR

Here, $G_F$ denotes the Fermi constant, $m_f$ the mass of the fermions, and $s_f$, $p_f$ are model dependent coupling constants.

In the case of the SM one has $s_f = 1$ and $p_f = 0$. In the minimal supersymmetric extension of the SM the parameters $s_f$ and $p_f$ may be expressed by two angles with $s_f = \cos\alpha/\sin\beta$, $p_f = \cot\beta = 1/x$ for $f = u, c, t$ and $s_f = -\sin\alpha/\cos\beta$, $p_f = \tan\beta = x$ for $f = d, s, b, e, \mu, \tau$ [2]. The parameter $x$ defines the ratio of the vacuum expectation values of the two Higgs doublets $x = \vartheta_2/\vartheta_1$. Restricting on Higgs masses far below the $W$-boson mass, $\alpha$ becomes equal to $-\beta$ and $s_f = p_f$. Further, in the case of the Peccei-Quinn type axions $p_f$ is the same as in the MSSM.

In the present paper the production and decay of light scalar and pseudoscalar particles will be investigated in a proton-iron beam dump experiment at the 70 GeV Serpukhov accelerator. Three processes are studied yielding production cross sections which allow a dedicated search for decay products of these particles:

(i) Coherent proton-nucleus scattering
(ii) Parton-parton interactions
(iii) Inital state soft bremsstrahlung

The corresponding Feynman graphs are given in Figs. 1a–c.

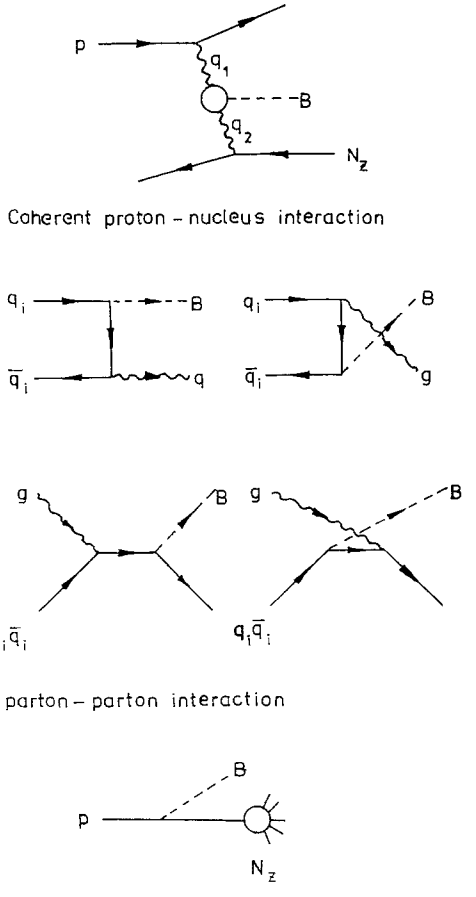


**Fig. 1a–c.** Lowest order Feynman diagrams including (pseudo)scalars; **a** coherent proton-nucleus scattering, **b** parton-parton interaction, **c** initial state soft bremsstrahlung

For the detection of possible pseudosclar or scalar particles the IHEP-JINR neutrino detector [10] is used. An iron shielding of 54 m length between the beam dump target and the detector prevents the penetration of all particles except neutrinos and weakly interacting neutral particles. A search is performed for electromagnetic decays into $\gamma\gamma$- and $e^+e^-$-pairs. Scalar and pseudoscalar particles with $M_{A,H} > 2m_\mu$ are too short-lived at our energy region and decay already before they can reach the detector. The $e^+e^-$- and $\gamma\gamma$-decays have a very clean signature of an isolated electromagnetic shower in beam direction in the fiducial volume of the detector. The different decay widths for the pseudoscalar and scalar particles are given in the Appendix A.

The paper is organized as follows. In Sect. 2 the experimental set up is described. In Sect. 3 data taking and the data analysis are summarized. Limits on masses and lifetimes for these particles are derived in Sect. 4 and are compared with results of other experiments. Section 5 contains the discussion. The production cross sections and the decay widths of scalar and pseudoscalar particles are given in the Appendix.

## 2 Experimental set up

A schematic view of the beam dump experiment is given in Fig. 2. The fast-ejected 70 GeV proton beam is guided to the beam dump target with help of the standard system for the wide band neutrino beam. The intensity of the proton beam is measured by two monitor counters installed in the proton beam line. To minimize the distance between target and detector, the iron beam dump is located directly in front of the muon shield. As shown in Fig. 2, two targets are used*. The density $\rho = 1$ target consists of an 140 cm iron block. In the $\rho = 1/2$ configuration 50 iron sheets of 1 cm thickness are arranged with an 1 cm air interspace betwen them and followed by a 90 cm iron block.

The iron muon shield has a length of 54 m. The total $\mu^\pm$-flux is measured in a region of 0.7 m radius around the beam axis in ten gaps located in the first 20 m of the shield. These data are taken for each proton pulse and allow an adjustment of the Monte Carlo simulation of the conventional muon neutrino fluxes.

The neutrino detector is located at a distance of 64 m down-stream of the beam dump. The target part of the detector consists of 36 modules with the following structure per module**:

- a magnetized iron frame for the muon momentum measurement
- an aluminium plate (5 cm) as neutrino target and shower absorber which fills the inner free space of $3 \times 3$ m$^2$ of the frame
- $x-y$ drift chamber planes of $4.5 \times 4.5$ m$^2$ for the track measurements in the target part and in the iron frame

* This configuration was applied for a search for prompt neutrinos from charm decays performed in the same exposure

** A detailed description of the detector is given in [10]

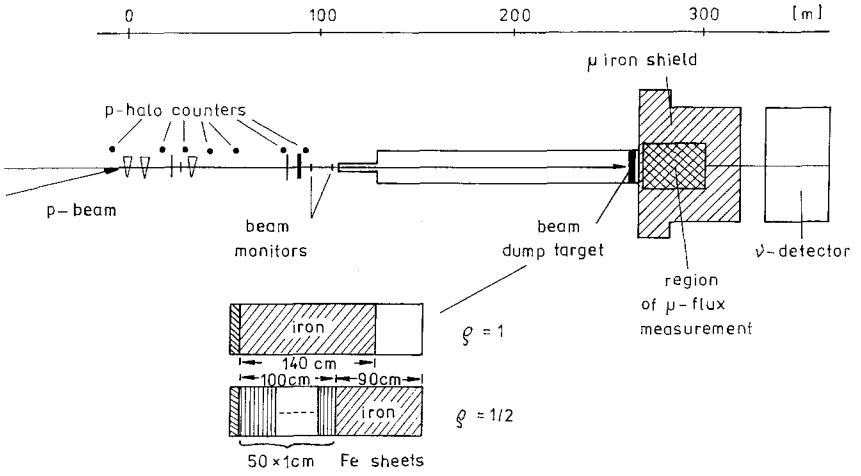


**Fig. 2.** Schematic view of the experimental arrangement

- a $CH_2$-liquid scintillator target calorimeter of 10 counters, each with the transversal dimension of $5 \times 0.3\ m^2$ and a thickness of 0.20 m, giving a sensitive plane of $5 \times 3\ m^2$.

For the beam dump experiment a fiducial volume of 30 detector modules is chosen, starting with the fourth module. The first three modules are used as veto counters for incoming charged particles. The fiducial plane has an extension of $2.6 \times 2.6\ m^2$. A plastic scintillator-lead sandwich detector of a depth of 10 radiation lengths measures electromagnetic shower leakage at the end of the target calorimeter. The last part of the neutrino detector consists of a muon spectrometer of magnetized iron toroids and $x-y$ drift chamber planes.

## 3 Data taking and analysis

In the total exposure the number of protons on target amounted to $1.71 \times 10^{18}$, with about 60% interactions in the $\rho = 1$ target. The average proton intensity per accelerator pulse was $1.21 \times 10^{13}$. The different types of dump targets do not influence the production spectra of the light scalar and pseudoscalar particles studied in the present investigation, because only direct production was considered. However, since two times more of the produced $\pi$- and $K$-mesons can decay at the $\rho = 1/2$ density, also the background of events in the detector induced by these conventional neutrinos is a factor of two higher than for the $\rho = 1$ exposure.

The signature of event candidates for weakly interacting neutral scalar or pseudoscalar particles which decay into $e^+e^-$- or $\gamma\gamma$-pairs consists of a single electromagnetic shower in the fiducial volume of the detector. The experimental arrangement does not allow to distinguish between the two decay channels since almost all of the gammas are produced overlapping in the forward direction.

The background comes from neutrino events with an electromagnetic shower but no visible muon track and rudimentary hadron shower activity. For the investigation of these background events detailed Monte Carlo studies were performed and compared with real events coming from charged and neutral current interactions of conventional neutrinos [11]. It is shown that the experimental data are very well described by the Monte Carlo program [12] using the beam dump neutrino spectra [13]. The event generator takes into account quasielastic [14], resonant [15] and deep inelastic reactions. The structure functions of the deep inelastic scattering cross section are described by the parton distributions [16] which are appropriate for the kinematical range $E_\nu < 30$ GeV. Furthermore, events due to coherent $\pi^0$-production [17] and $\overset{(-)}{\nu}\ e$-scattering were included.

The geometrical and kinematical data analysis was performed using the program GRAND [18] which allows the reconstruction of the vertex, the electromagnetic and hadronic showers and the muon track of events. GRAND is also used to calculate the reconstruction efficiencies for the signal and background processes, passing Monte Carlo events through the program.

The reconstruction of event candidates from the total exposure yields 3880 events with the vertex in the fiducial volume and with visible energy in the scintillator modules. To select candidates for weakly interacting neutral particles decaying into $e^+e^-$- or $\gamma\gamma$-pairs, we search for events with an electromagnetic shower and without a muon track or a hadronic shower.

The calibration of scintillation counters with electrons and hadrons at fixed beam energies as well as corresponding Monte Carlo studies have shown, that electromagnetic showers are characterized by high energy deposit in a narrow tube in the direction of the shower particle. For instance 5 GeV electrons produce electromagnetic showers with a mean half width of $34 \pm 4$ cm and an average range of 10 radiation lengths. If the energy exceeds 3 GeV, the reconstruction program can well distinguish electromagnetic from hadronic showers even if there is an overlap between both.

Requiring events with an electromagnetic shower of $E_{\text{elm}} > 3$ GeV, 106 events remain. A large fraction of them has an energetic hadron shower. This part can be removed by excluding all events with hadron energies above 1.5 GeV. For the remaining 21 events the electromagnetic shower energy is shown in Fig. 3a. The dotted curve represents the Monte Carlo background contribution obtained using the same cuts. The efficiency to reconstruct

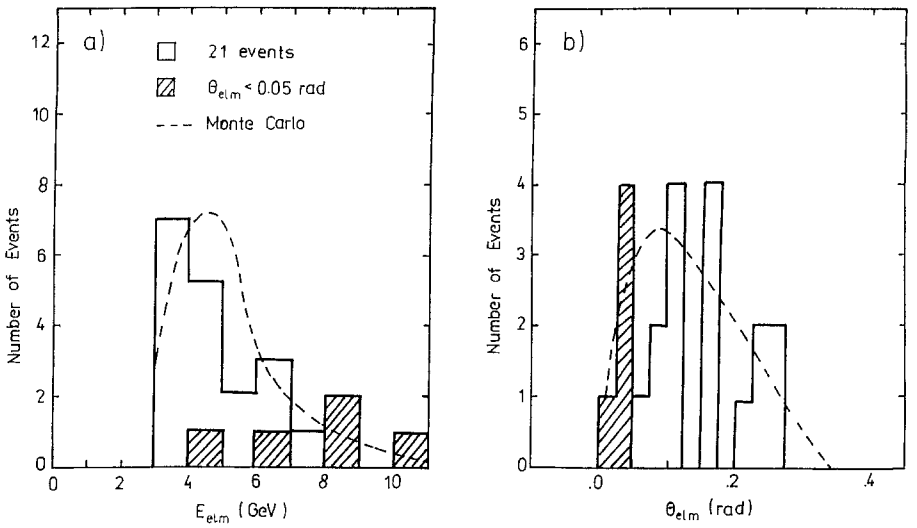


**Fig. 3.** Electromagnetic energy distribution of beam dump events without muon, with electromagnetic shower and a hadronic energy $E < 1.5$ GeV (full line: real data, dashed curve: Monte Carlo calculation of the background); the hatched histogram: real data with additional cut for production angle of electromagnetic shower $\Theta < 0.05$ rad

events with an electromagnetic shower amounts to 70%. About 2/3 of the background comes from $\overset{(-)}{\nu}_e N$-events with an $e^-(e^+)$, the rest from $\overset{(-)}{\nu}_\mu N$-events with a $\pi^0$ in the final state. Within the errors, the background expected from neutrino interactions is in good agreement with the experimental sample.

Particles produced in the beam dump cover a production angle of $\Theta \leqq 0.02$ rad at the detector position. In systematical Monte Carlo studies the reconstruction accuracy for the production angle of single electromagnetic showers was found to be $\sigma(\Theta) = 0.01$ rad. Figure 3b shows the production angle $\Theta_{\text{elm}}$ of the 21 events. Since the electromagnetic showers of the $e^+e^-$ and $\gamma\gamma$ decays of the light (pseudo) scalar particles are dominantly located in a forward angle $\Theta_{\text{elm}} < 0.05$ rad taking into account both the maximum shower angle and the reconstruction accuracy this cut was used to further reduce the background. There remain 5 events with a signature of an isolated electromagnetic shower. These events are shown in the hatched histograms of Fig. 3. The corresponding Monte Carlo background amounts to 3.5 neutrino events from the following sources: 3.0 charged current $\nu_e$-interactions, 0.3 events from deep inelastic and resonant $\pi^0$-production, 0.1 coherent $\pi^0$ events and 0.1 events from $\nu e$ elastic scattering. No excess over background was found.

## 4 Mass and lifetime limits

Different reactions may be considered as sources for long lived light scalars and pseudoscalars in the present experiment:

a) coherent $pA$-scattering producing these particles via $\gamma\gamma$-fusion;
b) parton-parton scattering and
c) initial state proton bremsstrahlung, where these particles are emitted collinearly of the proton hitting the dump target.

Using the relations summarized in Appendices B–D the light particle fluxes expected at the position of the detector were calculated as a function of the particle energy in the laboratory frame using $x = 1$ to determine the coupling strength. These fluxes are shown in Figs. 4a–c for the different reactions. For coherent $pA$-scattering and initial state proton bremsstrahlung the particle spectra are dominated by the low energy range. Contrary to this, parton-parton scattering at $p_t > 0.5$ GeV leads to a high energetic spectrum since only the forwardly produced particles can be detected.

The total number of possible decays of particles with the energy $E$ and mass $m$ is obtained by the following relation

$$\frac{\mathrm{d}N(E,m)}{\mathrm{d}E} = \Phi(E,m) \cdot N_p \cdot W(E,m) \cdot \varepsilon(E), \tag{4.1}$$

where $\Phi$ denotes the flux of the (pseudo)scalar particles per proton. $N_p$ is the total number of protons on target, $W(E,m)$ is the decay probability of the particles in the fiducial volume of the detector. Since the distance between target and detector is relatively small, the decay probability reaches values up to about 10%. $\varepsilon(E)$ is the reconstruction efficiency for an isolated electromagnetic shower of energy $E$ and amounts to about 70% independent of the energy.

For the derivation of the exclusion limits the $\chi^2$-method was used comparing the expected event numbers (4.1) with the difference of the measured spectra and the neutrino induced background. The analysis was performed for each of the above production processes separately.

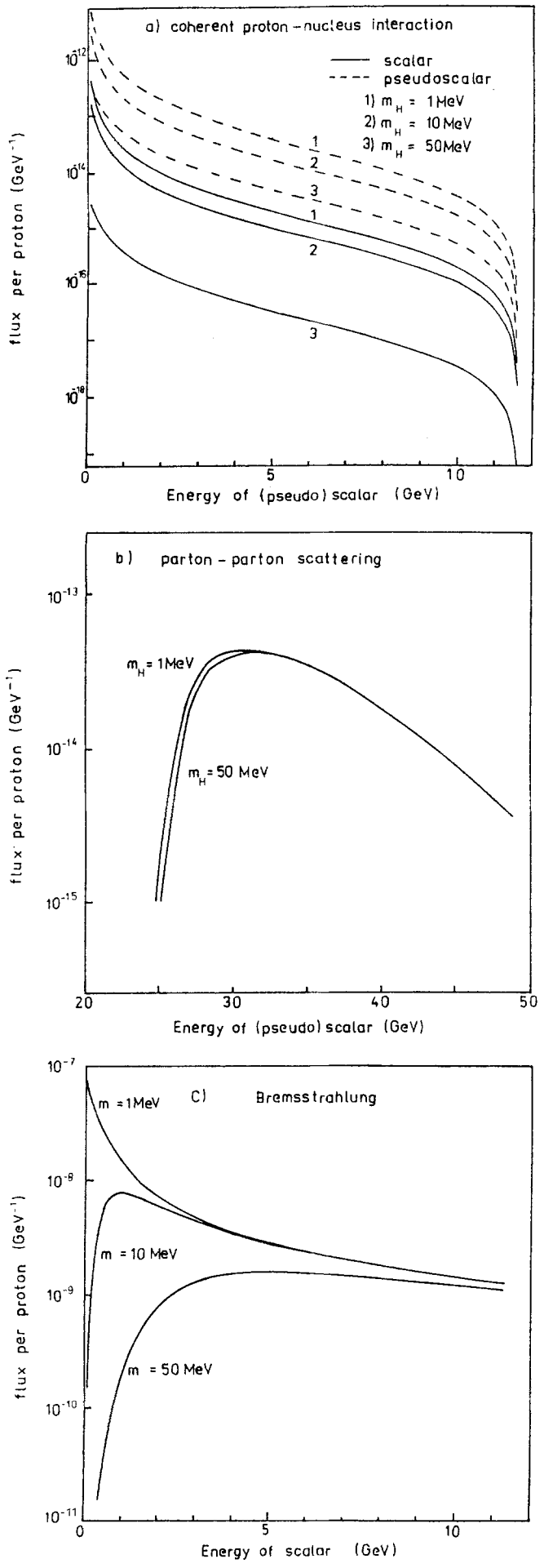


**Fig. 4a–c.** Flux per proton of (pseudo)scalar particles of the MSSM with $x=1$ in forward direction; **a** coherent proton-nucleus interaction, **b** parton-parton interaction, **c** initial state soft bremsstrahlung

Table 1 gives the 95% CL excluded mass ranges of the one parameter space ($m_H$) for the Higgs of the Standard Model.

**Table 1.** Exclusion of Standard Model Higgs

| Process | Excluded mass range |
|---|---|
| Coherent proton-nucleus interactions | $1 < m_H < 30$ MeV |
| Parton-parton interaction | $5 < m_H < 80$ MeV |
| Bremsstrahlung | $1 < m_H < 70$ MeV |

The 95% CL exclusion curves of the two parameter space ($m_{H,A}, x$) are shown in Fig. 5a for scalar and in Fig. 5b for pseudoscalar Higgs particles of the MSSM in dependence on the parameters $x$ versus mass. They are compared with the published result of an electron beam dump experiment [19].

Using the relations on the decay length it is straightforward to translate these curves into the mass-lifetime plots. The shape of the exclusion area is mainly determined by the decay probability. The upper end of the mass scale comes from the decreasing fluxes at higher energies and higher masses.

We also consider Peccei Quinn type axions which behave similar as a special case of the light pseudoscalar particle of the MSSM because $m_A$ and $x$ are related by

$$m_A = 52\,\text{keV} \cdot N_f (x + 1/x)\sqrt{z}/(1+z), \tag{4.2}$$

with $N_f = 3$ the number of fermion families and $z = 0.56$ [20] the ratio of the masses of $u$- and $d$-quark. Figure 6 shows the exclusion area of an light pseudoscalar particle in the $x - m_A$ plane where (4.2) was used to calculate the curve for the standard axion. Since this experiment is not sensitive to very light and longlived particles which escape detection before decaying, we can only exclude two separate regions for the standard axion above and below $x \approx 1$ which are given in Table 2.

## 5 Discussion

In a search for neutral weak interacting scalar and pseudoscalar particles produced in a proton-iron beam dump and decaying into $\gamma\gamma$- and $e^+e^-$-pairs, no signal over a background of neutrino events was observed. Limits were derived on the mass and lifetime of these particles in the frame of the Standard Theory, its supersymmetric extension and for Peccei-Quinn type axions.

For the Higgs particle of the Standard Model mass regions

$1 < m_H < 30$ MeV (coherent proton-nucleus interactions)

**Table 2.** Exclusion of Peccei-Quinn like axions

| Process | $x>1$ | $x<1$ |
|---|---|---|
| Coherent proton-nucleus interactions | 0.6 MeV $< m <$ 2.0 MeV<br>8.2 $< x <$ 26 | 0.6 MeV $< m <$ 8.0 MeV<br>0.01 $< x <$ 0.12 |
| Parton-parton interactions | 0.7 MeV $< m <$ 3.2 MeV<br>9.0 $< x <$ 40 | 1.3 MeV $< m <$ 11.0 MeV<br>0.007 $< x <$ 0.075 |
| Bremsstrahlung | 0.2 MeV $< m <$ 2.5 MeV<br>1.3 $< x <$ 32 | 0.2 MeV $< m <$ 9.2 MeV<br>0.008 $< x <$ 0.7 |

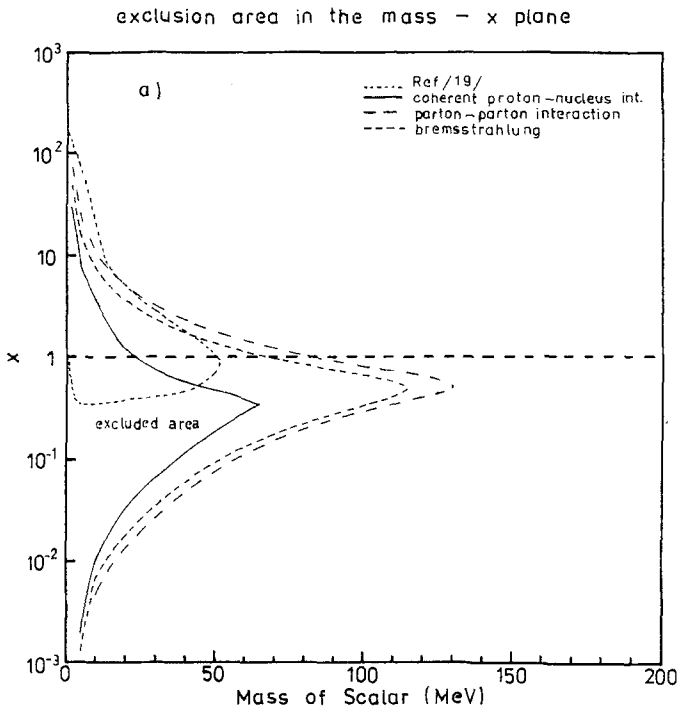


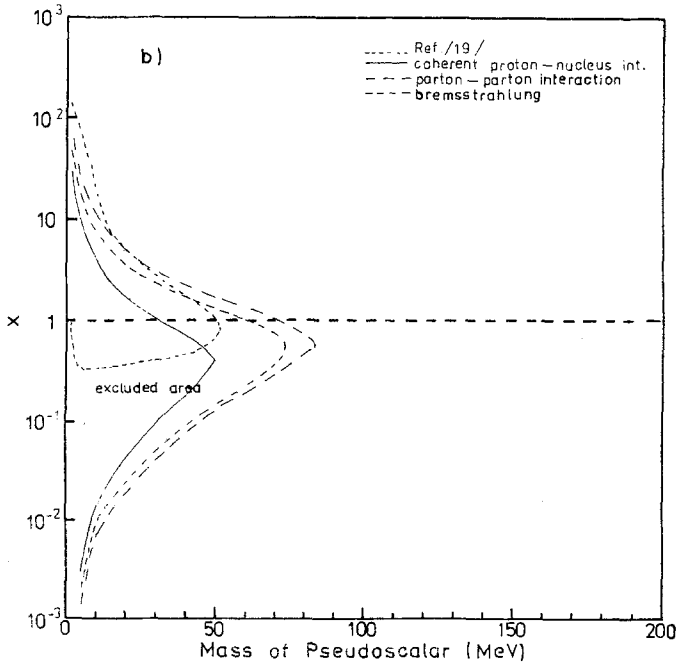


**Fig. 5a, b.** **a** Exluded area for the light scalar of the MSSM. **b** Excluded area for the light pseudoscalar of the MSSM

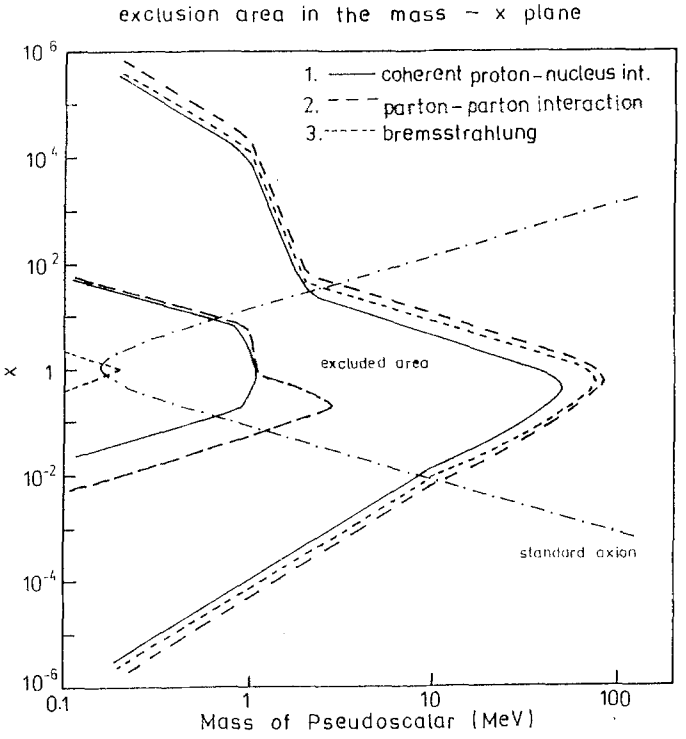


**Fig. 6.** Excluded area for Peccei Quinn Axion in the $x$-mass plane

$5 < m_H < 80$ MeV (parton-parton interactions)

$1 < m_H < 70$ MeV (bremsstrahlung)

are excluded at 95% CL.

Similar results were obtained in an electron beam dump experiment [19] and by the SINDRUM experiment [21], which excluded the mass region 1.2–52 MeV and 10–100 MeV respectively. Recently the Crystal Ball Collaboration [22] ruled out masses below 86 MeV.

For the two light members of the Higgs family of the supersymmetric extension of the Standard Model the range in the $m-x$-plane which was excluded in the $e^-$-beam dump experiment [19] is extended by our measurement towards higher masses both for scalar and pseudoscalar particles. These values correspond to exclusions of the mass ranges

$m_{sc} < 120$ MeV at 95% CL for $\tau_{sc} = 10^{-10}$ s

$m_{ps} < 80$ MeV at 95% CL for $\tau_{ps} = 4 \times 10^{-11}$ s.

For Peccei-Quinn axions the limits are summarized in Table 2 depending on the production process. They confirm the results obtained by earlier experiments.

In the present experiment mainly the coupling of light scalars and pseudoscalars to the light fermions $e, u, d, s$ was probed. Complementary to this, searches for these particles at LEP are mainly sensitive to the $ZZH$-coupling. Very recently different experimens have excluded the mass range $M_H < 41$ GeV [23].

## Appendix A

*Decay length of a (pseudo)scalar particle due to the decay channels $H(A) \to e^+ e^-$ and $H(A) \to \gamma\gamma$*

The decay lengths of a scalar and pseudoscalar particle in the two relevant channels are given by [8, 24]*

$$\lambda(H \to \gamma\gamma) = \frac{64\pi^3}{\alpha^2 \sqrt{2}\, G_F m_H^3} \times \left| \tfrac{2}{3} \sum_f Q_f^2 C_f I_H(m_f^2/m_H^2) s_f - \tfrac{7}{2} s_W \right|^{-2}, \tag{A.1}$$

$$\lambda(A \to \gamma\gamma) = \frac{64\pi^3}{\alpha^2 \sqrt{2}\, G_F m_A^3} \times \left| \sum_f Q_f^2 C_f I_A(m_f^2/m_A^2) p_f \right|^{-2}, \tag{A.2}$$

$$\lambda(H \to e^+ e^-) = \frac{8\pi}{\sqrt{2}\, G_F m_H m_e^2 s_e^2} \times [1 - 4m_e^2/m_H^2]^{-3/2}, \tag{A.3}$$

$$\lambda(A \to e^+ e^-) = \frac{8\pi}{\sqrt{2}\, G_F m_A m_e^2 p_e^2} \times [1 - 4m_e^2/m_A^2]^{-1/2}, \tag{A.4}$$

where $Q_f$ denotes the fermion charge, $C_f$ is the corresponding color factor and $I(z)$ describes a complex function defined by

$$I_H(z) = 3 \int_0^1 \mathrm{d}x \int_0^{1-x} \mathrm{d}y \, \frac{1 - 4xy}{1 - xy/z}; \tag{A.5}$$

$$I_A(z) = 2 \int_0^1 \mathrm{d}x \int_0^{1-x} \mathrm{d}y \, \frac{1}{1 - xy/z}; \tag{A.6}$$

with $I_{H,A}(z) \to 1$ for $z \to \infty$. $s_f$ and $p_f$ were introduced above in connection with (1.1, 2).

From [2] one obtains $s_W = 2x/(1+x)^2$ for the $W$-boson loop in the MSSM. Covering all characteristics of the Higgs sector of the MSSM one has also to take into account loops from charged Higgs bosons, calculating (A.1). Because $m_{H^\pm} > m_W$ (cf. [2]) the effect due to these loops leads to a replacement of 7/2 by $(7/2 - m_W^2/6m_{H^\pm}^2)$ in (A.1). The term is supressed if $m_{H^\pm}$ becomes large, if $x$ differs remarkably from 1 or if the $e^+e^-$ decay channel becomes important. We checked that the influence of the $H^\pm$ loop on our results is negligibly small even if one assumes $m_{H^\pm} = m_W$ yielding the maximal contribution.

* We have not considered QCD-corrections calculating the $\gamma\gamma$-decay width. These contributions are not yet evaluated for the range of small Higgs masses, but could be important as argued in a recent pertubative calculation [25] for higher Higgs masses

## Appendix B

*Production of scalar and pseudoscalar particles in coherent proton-nucleus interaction*

In the two-photon production of scalar and pseudoscalar particles via coherent proton-nucleus interactions as shown in Fig. 1a the scattering partners react elastically. The advantage of this process is the absence of ambiguities due to hadronic effects because the reaction can be described in the Weizsäcker-Williams approximation (WWA) [26]. The WWA is valid in the range $-q^2 \ll W^2$ which means that the virtual photon mass has to be small compared with the mass of the $\gamma\gamma$-system. Since our investigation covers the range $W^2 = M_{H,A}^2 \leqq (100\ \mathrm{MeV})^2$, the nuclei can be taken as pointlike charges because the virtual photon mass does not exceed the inverse nuclear radius

$$q^2 < R_i^{-2}, \quad \text{with} \tag{B.1}$$

$$R_i = R_0 A^{1/3}; \quad R_0 = 1.2\text{–}1.4\ \mathrm{fm}.$$

Using the formalism of the WWA the cross section factorizes as [27]

$$\frac{\mathrm{d}\sigma}{\mathrm{d}W^2}(pN_z \to pN_z X) = \frac{\mathrm{d}L_{\gamma\gamma}}{\mathrm{d}W^2} \hat{\sigma}(\gamma\gamma \to X). \tag{B.2}$$

$L_{\gamma\gamma}$ is the two-photon luminosity, $W$ the mass of system $X$ and $\hat{\sigma}$ the real two-photon production cross section of system $X$. Neglecting the virtual photon mass and any transverse momentum one obtains

$$W^2 = 4\omega_1\omega_2, \tag{B.3}$$

and

$$\frac{\mathrm{d}L_{\gamma\gamma}}{\mathrm{d}W^2} = \left(\frac{2}{\pi} Z\alpha\right)^2 \iint \frac{\mathrm{d}\omega_1\, \mathrm{d}\omega_2}{\omega_1\omega_2} \ln\left[\frac{\gamma_1}{\omega_1 R_1}\right] \times \ln\left[\frac{\gamma_2}{\omega_2 R_2}\right] \delta(W^2 - 4\omega_1\omega_2), \tag{B.4}$$

with $\omega_i$ the c.m.s. energy of the photon $i$, $\gamma_i = E_i^{\mathrm{cm}}/M_i$ and $Z$ the charge of the nucleus. The integrals are bounded by the conditions (B.5) resulting from (B.1) and (B.3)

$$\omega^- < \omega_1 < \omega^+, \quad \text{with}$$

$$\omega^+ = \gamma_1/R_1, \qquad \omega^- = R_2 W^2/(4\gamma_2). \tag{B.5}$$

For $\omega_2$ the upper and lower limits $\omega^+$, $\omega^-$ are obtained by exchanging the indices 1 and 2.

The real two-photon production cross section of a scalar or pseudoscalar particle of mass $M_{H,A}$ is then

$$\hat{\sigma}(\gamma\gamma \to H, A) = 8\pi^2 \frac{\Gamma(H, A \to \gamma\gamma)}{M_{H,A}} \delta(W^2 - M_{H,A}^2). \tag{B.6}$$

The decay widths of a scalar and pseudoscalar particle into two $\gamma$ are given in (A.1, 2). Using (B.4) and (B.6) to calculate (B.2) and integrating both $\delta$-functions one gets

$$\sigma(pN_z \to pN_z H, A) = 32(Z\alpha)^2 \frac{\Gamma(H, A \to \gamma\gamma)}{M_{H,A}^3} \times \int \frac{d\omega_1}{\omega_1} \ln\left[\frac{\omega^+}{\omega_1}\right] \ln\left[\frac{\omega_1}{\omega^-}\right]. \tag{B.7}$$

To obtain the differential cross section with respect to $E_{H,A}^{\text{lab}}$ we have to transform $\omega_1$.

$$E_{H,A}^{\text{cm}} = \omega_1 + \omega_2 = \omega_1 + M_{H,A}^2/(4\omega_1), \tag{B.8}$$

which gives

$$\omega_{1,2} = \tfrac{1}{2}(E_{H,A}^{\text{cm}} \pm p_{H,A}^{\text{cm}}), \tag{B.9}$$

where the plus sign refers to the photon coming from the beam which we will define to have the energy $\omega_1$ and the minus sign refers to the photon coming from the target with energy $\omega_2$. Transformed into the laboratory system we get

$$\omega_{1,2} = \tfrac{1}{2}(E_{H,A}^{\text{lab}} \pm p_{H,A}^{\text{lab}}) \times (E_1^{\text{lab}} + M_2 \mp p_1^{\text{lab}}) \frac{1}{\sqrt{s}}, \tag{B.10}$$

with

$$M_1 = m_p$$

$$M_2 = 56\, m_p \quad \text{(Fe target)},$$

which for $E_{H,A}^{\text{lab}} \gg M_{H,A}$ and $E_1^{\text{lab}} \gg M_1$ simplifies to

$$\omega_1 = E_{H,A}^{\text{lab}} \times M_2/\sqrt{s}, \qquad \omega_2 = \frac{M_{H,A}^2}{4E_{H,A}^{\text{lab}}} \times \sqrt{s}/M_2. \tag{B.11}$$

Using (B.11) one obtains from (B.7) the differential cross section

$$\frac{d\sigma}{dE_{H,A}} = 32(Z\alpha)^2 \frac{\Gamma(H, A \to \gamma\gamma)}{M_{H,A}^3} \frac{1}{E_{H,A}} \times \ln\left[\frac{\omega^+ \sqrt{s}}{E_{H,A} M_2}\right] \ln\left[\frac{E_{H,A} M_2}{\omega^- \sqrt{s}}\right]. \tag{B.12}$$

This leads to an upper bound for $E_{H,A}$:

$$E_{H,A} < \frac{\omega^+ \sqrt{s}}{M_2} = \frac{E_1^{\text{cm}} \sqrt{s}}{M_1 M_2 R_1} \approx 12\ \text{GeV}. \tag{B.13}$$

The fluxes calculated from (B.12) for several values of $M_{H,A}$ are shown in Fig. 4a.

## Appendix C

*Calculation of the cross section of scalar and pseudoscalar particles in parton-parton interaction*

The production of light (pseudo)scalar particles in hard proton-nucleon collisions can be described by the quark-antiquark annihilation process and by quark-gluon compton scattering shown in the diagrams of Fig. 1b using the parton model. The cross section for partons of fractional momenta $x_1$ and $x_2$ of the nucleon 1 and 2 is given by

$$\frac{d\sigma}{dx_1 dx_2 dE_H} = \frac{1}{\Delta E_H} \sum_i \left\{ [f_{i1} \bar{f}_{i2} + f_{i2} \bar{f}_{i1}] \times \int_{\hat{t}_{\min}}^{\hat{t}_{\max}} \frac{d\sigma_{Ai}(\hat{s}, \hat{t})}{d\hat{t}} d\hat{t} + [G_1(f_{i2} + \bar{f}_{i2}) + G_2(f_{i1} + \bar{f}_{i1})] \times \int_{\hat{t}_{\min}}^{\hat{t}_{\max}} \frac{d\sigma_{Ci}(\hat{s}, \hat{t})}{d\hat{t}} d\hat{t} \right\}. \tag{C.1}$$

$\overset{(-)}{f}_{ij} = \overset{(-)}{f}_i(x_j, Q^2)$ are the quark and antiquark distributions in a proton and $G_j(x_j, Q^2)$ denotes the gluon distribution function with $Q^2 = \hat{s}$, $\hat{s}$ and $\hat{t}$ are Mandelstam variables of the parton subsystem. $\hat{t}_{\min}$ and $\hat{t}_{\max}$ are functions of $\Theta_{\max}$ and $E_H \cdot \Theta_{\max} = 1,2°$ is the maximum polar angle in the laboratory frame defined by the geometrical acceptance of our detector. $E_H$ is the energy of the (pseudo)scalar particle in the laboratory frame. $\hat{s}$ is related to the center of mass energy of the nucleon system by

$$\hat{s} = x_1 x_2 (s - 2M_N^2) + m_1^2 + m_2^2, \tag{C.2}$$

where $M_N$ denotes the nucleon mass and $m_1$, $m_2$ are the masses of the two initial partons.

The differential cross section $d\sigma/d\hat{t}$ were calculated using REDUCE [28].

$$\frac{d\sigma_{Ci}(\hat{s}, \hat{t})}{d\hat{t}} = \tfrac{1}{6} \frac{\alpha_s}{4} g_H^2 \lambda^{-1}(\hat{s}, m^2, 0) \times \left\{ -\frac{\hat{u} - m_i^2}{\hat{s} - m_i^2} - \frac{\hat{s} - m_i^2}{\hat{u} - m_i^2} - 2 - a\left[\frac{\hat{t}}{(\hat{s} - m_i^2)(\hat{u} - m_i^2)} - m_i^2 \left[\frac{1}{(\hat{s} - m_i^2)} + \frac{1}{(\hat{u} - m_i^2)}\right]^2\right]\right\}, \tag{C.3}$$

$$\frac{d\sigma_{Ai}(\hat{s},\hat{t})}{d\hat{t}} = -\frac{4}{9}\frac{\alpha_s}{4} g_H^2 \lambda^{-1}(\hat{s}, m^2, m^2) \times \left\{ -\frac{\hat{u}-m_i^2}{\hat{t}-m_i^2} - \frac{\hat{t}-m_i^2}{\hat{u}-m_i^2} - 2 - a\left[\frac{\hat{s}}{(\hat{t}-m_i^2)(\hat{u}-m_i^2)} - m_i^2\left[\frac{1}{(\hat{t}-m_i^2)} + \frac{1}{(\hat{u}-m_i^2)}\right]^2\right]\right\}, \quad \text{(C.4)}$$

where $m_i$ denotes the quark mass, $\hat{u} = 2m_i^2 + m_H^2 - \hat{s} - \hat{t}$ and the triangle function is given by $\lambda(a,b,c) = a^2 + b^2 + c^2 - 2ab - 2ac - 2bc$. $g_H$ denotes the coupling of the (pseudo)scalar to the quark as defined at (1.1, 2). The parameter $a$ is a function of the quark mass $m_i$ and the mass of the (pseudo)scalar $m_H$ and differs for scalar and pseudoscalar particles.

$$\begin{aligned} a &= 2m_H^2(1 - 4m_i^2/m_H^2) \quad \text{scalar}, \\ a &= 2m_H^2 \quad \text{pseudoscalar}. \end{aligned} \quad \text{(C.5)}$$

$d\sigma_{Ai}/d\hat{t}$ is obtained from $d\sigma_{Ci}/d\hat{t}$ by crossing symmetry $\hat{s} \leftrightarrow \hat{t}$ for the matrix element up to different color factors. In the massless case $m_i \to 0$, $d\sigma_{A,C}/d\hat{t}$ become identical for the production of scalars and pseudoscalars. The integration over $\hat{t}$ can be carried out analytically because we have chosen $Q^2 = \hat{s}$ as the scale of the parton distributions.

To cut out the soft region where higher order QCD contributions become sizeable, a transverse momentum cut of $p_t > 0.5$ GeV was applied. Because of large contributions to the cross sections from the low $\hat{s}$ range, $\alpha_s$ is defined for $Q^2 < Q_0^2 = 4\,\text{GeV}^2$ by $\alpha_s(Q_0^2)$ to avoid unnatural high contributions in a range where higher order QCD-contributions are getting large. We also do not account for a contribution due to the Bjorken-Weisberg [29] enhancement to give conservative bounds for the masses and lifetimes.

For the calculation of the production cross section we use the parametrization of the parton distributions by Duke and Owens [30] for $\Lambda = 200$ MeV, $N_f = 4$ and the quark masses [20] $m_u = 4.2$ MeV, $m_d = 7.5$ MeV, $m_s = 150$ MeV, $m_c = 1200$ MeV. To study the influence of the structure function on the flux the calculation is also done with a structure function set given in [31]. The agreement between the resulting fluxes is within 20%. Finally the flux is shown in Fig. 4b in dependence on the energy of the (pseudo)scalar particle. Differences between scalar and pseudoscalar particles turn out to be very small (cf. Fig. 4b).

## Appendix D

*Production of scalar and pseudoscalar particles due to initial state soft bremsstrahlung*

If the mass of the scalar or pseudoscalar particle fulfills the condition

$$M_{H,A} < 1/R, \quad \text{(D.1)}$$

it can couple coherently to a nucleus of radius $R$. For the proton (D.1) restricts the mass of the scalar or pseudoscalar particle to values smaller than 150 MeV which agrees with the search limit given by the experimental arrangement and the decay length.

In the soft limit, i.e. $E_{H,A} \ll E_p = 70$ GeV, the bremsstrahlung cross section for the Higgs from the Standard Model is given by [32]

$$\sigma^H(p,k) = 4g_H^2 M_p^2 \times \int \frac{d^3\vec{k}}{(2\pi)^3 2k_0 [M_H^2 - 2(pk)]^2} \times \sigma_{\text{tot}}(p\,\text{Fe}), \quad \text{(D.2)}$$

with $g_H$ the Higgs-proton coupling, $M_p$ the mass, $p$ the four momentum of the proton, $M_H$, $k$ the mass, four momentum of the Higgs and $\sigma_{\text{tot}}(p\,\text{Fe}) = 1120$ mbarn.

The definition of $g_H$ includes some theoretical ambiguity because the proton cannot be treated as a fundamental fermion in the Standard Model a priori. $g_H$ has to be calculated from the coupling to the constituents of the proton. These aspects are discussed in [33] in detail. The error in the calculation of $g_H$ is estimated to be one order of magnitude. Taking into account this error, the upper bound of the mass of the Higgs from Standard Model has an uncertainty in the range of only 5 MeV because this bound is mainly influenced by the decay length. We follow this calculation and obtain

$$g_H = \tfrac{2}{27}\, n_H (\sqrt{2}\, G_F)^{1/2} M_p, \quad \text{(D.3)}$$

where $G_F$ denotes the Fermi constant and $n_H$ the number of heavy quarks because the main contribution to $g_H$ comes from gluon-gluon fusion via a heavy quark loop with $n_H = 3$.

From (1.1), (1.2) and the formulae of the $\gamma\gamma$-decay length (A.1), (A.2) it is easy to extend the validity of (D.3) on scalar particles of the MSSM [2]. One has to replace

$$n_H \to x + 2/x, \quad \text{(D.4)}$$

where $x$ counts for the $b$-quark and $1/x$ for $c$ and $t$. Comparing the formulae for the $\gamma\gamma$-decay length of scalar and pseudoscalar particles and taking into account the gluon-photon analogy we can extend the validity of (D.3) to pseudoscalar particles of the MSSM by an additional factor 3/2 in the limit $M_{H,A} \ll m_q$. This is obviously fulfilled in our case for $q = c$, $b$, t.

To obtain the energy dependend flux of the scalar and pseudoscalar particles we have to integrate over the two angles taking into account the geometrical acceptance of the detector ($\Theta_{\max} = 1.2°$).

$$\frac{d\sigma^H}{dE_H} = \frac{1}{2\pi^2} g_H^2 M_p^2 \sigma_{tot} k I(E_H),$$

$$I = \int_a^1 \frac{d(\cos\theta)}{[M_H^2 - 2E_H E_p + 2kp\cos\theta]^2}, \quad \text{(D.5)}$$

$$I = \tfrac{1}{4}(1-a)/[\tfrac{1}{4} M_H^4 + M_p^2 E_H^2 - p^2 M_H^2 a - M_H^2 E_p E_H + (1+a)p(\tfrac{1}{2} M_H^2 k - E_p E_H k + p E_H^2)],$$

with

$$a = \cos(\Theta_{max}).$$

Because of the Lorentz boost the angular cut diminishes $\sigma$ by less than a factor two. The flux per proton calculated from (D.5) for a scalar particle with $x = 1$ (Higgs of the Standard Model) is shown on Fig. 4c. The energy range is limited by the validity condition of the soft bremsstrahlung approximation

$$E_H < \gamma / R_p = E_p/(M_p R_p) \approx 12\,\text{GeV}. \quad \text{(D.6)}$$

*Acknowledgements.* We would like to thank Chr. Wetterich, P. Yepes and P.M. Zerwas for discussions.

## References


1. P.W. Higgs: Phys. Rev. Lett. 12 (1964) 132; 13 (1964) 508; Phys.Rev. 145 (1966) 1156; F. Englert, R. Brout: Phys. Rev. Lett. 13 (1964) 321; G.S. Guralnik, C.R. Hagen, T.W.B. Kibble: Phys. Rev. Lett. 13 (1965) 585
2. J.F. Gunion, H.E. Haber: Nucl. Phys. B272 (1986) 1; J.F. Gunion, H.E. Haber: Nucl. Phys. B278 (1986) 449
3. R.D. Peccei, H.R. Quinn.: Phys. Rev. Lett. 38 (1977) 1440; Phys. Rev. D16 (1977) 1791
4. G. t'Hooft: Phys. Rev. Lett. 37 (1976) 8; Phys. Rev. D14 (1976) 3432
5. A.N. Vainshtein, V.N. Zakharov, M.A. Shifman: Usp. Fiz. Nauk, 131 (1980) 537; Sov. Phys. Usp. 23 (1980) 429
6. J.E. Kim: Phys. Rep. 150 (1987) 1; R.D. Peccei: DESY, 88-109 and: CP-violation, p. 503. C. Jarlskog (ed.). Singapore: World Scientific, 1990
7. J.F. Gunion, H.E. Haber, G.L. Kane, S. Dawson: The Higgs Boson Hunters guide, SCIPP-89/13, BNL-41644, UCD-89-4, June 1989
8. R.N. Cahn: Rep. Progr. Phys. 52 (1989) 389
9. S. Raby, G.B. West, C.M. Hoffmann: Phys. Rev. D39 (1989) 828
10. L.S. Barabash et al.: Proc. Int. Conf. Neutrino 1982, Balatonfuered, Hungary, 1982, Vol. 2, p. 249
11. J. Blümlein et al., Berlin-Budapest-Dubna-Serpukhov Coll.: $\nu$-CAL-Note 01-11-89; $\nu$-CAL-Note 05-12-89
12. J. Blümlein: $\nu$-CAL-Note 01-07-89
13. Yu.M. Sapunov: Program for the calculation of neutrino spectra in $p$-beam dumps, ONF, IHEP Serpukhov, unpublished
14. J. Ellis: Phys. Rep. C3 (1972) 261
15. D. Rein,. L.M. Sehgal: Ann. Phys. (New York) 133 (1981) 79
16. R.D. Field, R.P. Feynman: Phys. Rev. D15 (1977) 2590
17. D. Rein, L.M. Sehgal: Nucl. Phys. B223 (1983) 89
18. T.K. Koroljew et al.: Serpukhov preprint 89-100 (1989); T.K. Koroljew et al.: Serpukhov preprint 90-82 (1990)
19. M. Davier, H. Nguyen Noc: Phys. Lett. 229B (1989) 150
20. S. Weinberg: Festschrift for I.I. Rabi, L. Motz (ed.). New York: New York Academy of Science 1978
21. S. Egli et al.: Phys. Lett. 229B (1989) 533
22. D. Antreasyan et al., Crystal Ball Coll.: Phys. Lett. 251B (1990) 204
23. M.Z. Akrawy et al. (OPAL): Phys. Lett. 251B (1990) 211; M.Z. Akrawy et al. (OPAL): CERN-PPE/90-116 (1990); B. Adeva et al. (L3): Phys. Lett. 251B (1990) 311; B. Adeva et al. (L3): L3 Preprint #15 (1990); B. Adeva et al. (L3): L3 Preprint #19 (1990); P. Abreu et al. (DELPHI): Nucl. Phys. B342 (1990) 1; P. Abreu et al. (DELPHI): Phys. Lett. 245B (1990) 276; D. Decamp et al. (ALEPH): Phys. Lett. 236B (1990) 233; D. Decamp et al. (ALEPH): Phys. Lett. 237B (1990) 291
24. B. Lautrup, P. Olesen: Phys. Lett. 22 (1966) 342
25. Han-qing Zheng, Dan-di Wu: Phys. Rev. D42 (1990) 3760
26. E.J. Williams: K. Dan. Vidensk. Selsk. Mat. Fys. Medd. N4 (1935) 13; C.F. von Weizsäcker: Z. Phys. 88 (1934) 612
27. E. Papageorgiu: Phys. Rev. D40 (1989) 92; E. Papageorgiu: Phys. Lett. 250B (1990) 155; G. Baur, L.G.F. Filho: KFA Jülich Preprint 90-8313
28. A.C. Hearn: REDUCE User Manual, Version 3.2, The Rand Corporation, Santa Monica (1985)
29. J.D. Bjorken, H. Weisberg: Phys. Rev. D 13 (1976) 1405
30. D.W. Duke, J.F. Owens: Phys. Rev. D30 (1984) 49
31. J. Pakvasa et al.: Phys. Rev. D10 (1974) 2124
32. J. Ellis, M.K. Gaillard, D.V. Nanopoulos: Nucl. Phys. B106 (1976) 292
33. E. Papageorgiu: MPI-PAE/PTh 68/89 (1989)